Volume 47 http://acousticalsociety.org/

ICUA2022 International Conference on Underwater Acoustics
Institute of Acoustics

International Conference on Underwater Acoustics
Southampton, UK
20-23 June 2022

Computational Acoustics: Target Echo Strength - Measurements and Modelling

Photogrammetry as a finite element modelling geometry builder

Jake Kent and Aidan Burt
Department of Research & Innovation, ATLAS ELEKTRONIK GmbH, Dorchester, Dorset, DT2 8ZB, UNITED KINGDOM; jake.kent@uk.atlas-elektronik.com; jakekent1996@live.co.uk; aidan.burt@uk.atlas-elektronik.com

An ever evolving seabed object hazard means that maritime forces often need to quickly and accurately respond to unexpected encountered situations. This paper describes how photogrammetry of encountered objects can be rapidly assimilated into wideband sonar systems using simulated insonification data, enabling them to counter new objects.

Published by the Acoustical Society of America

 https://doi.org/10.1121/2.0001611

1. INTRODUCTION

The use of multi-physics simulation software, such as finite-element analysis, is ever increasing as the capability broadens and computing power increases. This software is often used in the maritime domain to generate synthetic vessel signature data or the acoustic response from a mine or mine-like object. As the physics captured by multi-physics simulation packages becomes more sophisticated, there is a growing need to apply these methods to more geometrically complex objects, particularly in the underwater defence domain, where objects are designed to attempt to emulate the chaotic geometry of nature as a form of obfuscation and camouflage.

2. PHOTOGRAMMETRY MODELLING

Generating a viable 3D model for FE analysis using photogrammetry has 4 main steps. Creating a suitable image dataset, generating a model via photogrammetry, simplifying the model complexity and finally conversion to a CAD file type. This section covers each of these steps individually.

A. PHOTOGRAPHY

Creating a 3D model via photogrammetry requires a large image dataset (30+) that clearly captures the entirety of the target object at a fixed distance at consistent angular intervals that ensure overlap, culminating in a dataset that fully encompasses the target object. This process may be repeated at several fixed distances in order to build a dataset that captures the most detail. See Figure 1 [1].

Figure 1. Photography technique for dataset capture [1]

If practicable, using soft ambient light reduces the effect of shadows, allowing for the greatest amount of detail to be captured. Video snapshots ensure overlap but at the cost of lower resolution.

For use in COMSOL, the inherent need for a high performance camera is reduced, as the model complexity must first be simplified prior to import. To demonstrate the capability with low specification hardware, the datasets used in this report were captured with a Google Pixel 3A, which sports a 1/2.6 inch 12.2 MP sensor with an f/1.8 aperture. In addition, the lighting in this dataset is not ideal but the technique, primarily the software 3DF Zephyr, is robust enough to generate a viable model from poor datasets. Figure 2 shows some examples of the image dataset used to generate the model discussed in this paper.

Figure 2. Image dataset example for rock model

B. PHOTOGRAMMETRY GEOMETRY BUILDER

The software, 3DF Zephyr, requires an input of an image dataset and can output a model at various stages of development, as either a point cloud or mesh. This software package has several parameters and tools that can be used to fine tune the photogrammetry modelling process to the type of model being developed. The development stage of interest for this technique is the first mesh stage, at which the model can be exported as a .STL file type. It's at this stage that the model is cropped out of its surrounding environment using the bounding box tool, as the photogrammetry process captures the entire scene so the model must be manually isolated before progressing to the geometry simplification process (see Figure 3). Additionally, if the dataset was not fully complete, 3DF Zephyr allows for any geometry holes to be patched (see Figure 4), which is typically the case for the underside of the object if the object was not lifted during the dataset recording.

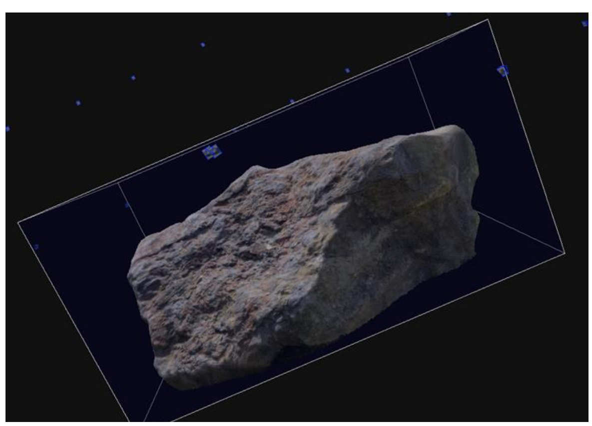

Figure 3. Cropped rock model within 3DF Zephyr

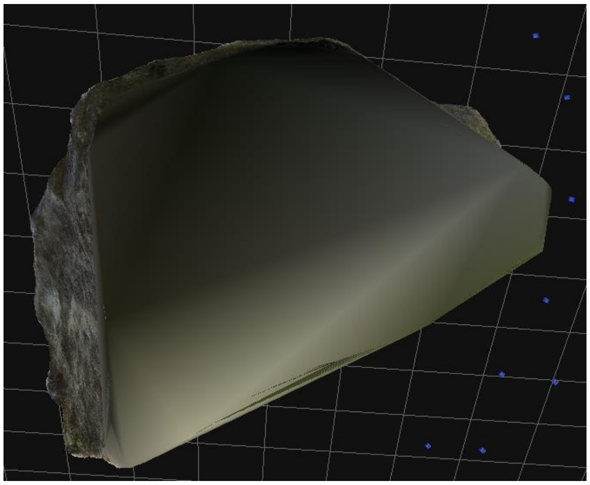

Figure 4. Patching the underside section of object

C. MODEL SIMPLIFICATION & OPTIMIZATION

The limiting factor in this process is the import function in COMSOL, the achieved fidelity discussed in this report has been optimized to produce the greatest fidelity that COMSOL allows without producing a fatal error upon import.

To reduce the complexity of the model, Blender's re-mesh and decimation tool is used to generate an optimized mesh established from a .STL file produced from 3DF Zephyr and to reduce the number of mesh elements respectively. The re-mesh tool allows for much greater fidelity than what is accepted into COMSOL, equal to the complexity of the original .STL model, and produces a more efficient model with optimized geometry and mesh elements. The decimate feature allows for slightly greater complexity if the object is complex and awkwardly shaped at a cost of reducing the number of mesh elements, requiring a fine balance between the 2 tools to create an efficient but still complex mesh. It is at this stage that a specified shell thickness may be applied, or alternatively, the model can be edited to be completely solid, as the output from 3DF Zephyr is a thin shell of the object. Once the object model has been sufficiently represented and optimized, the model is exported as a .STL file (see Figure 5).

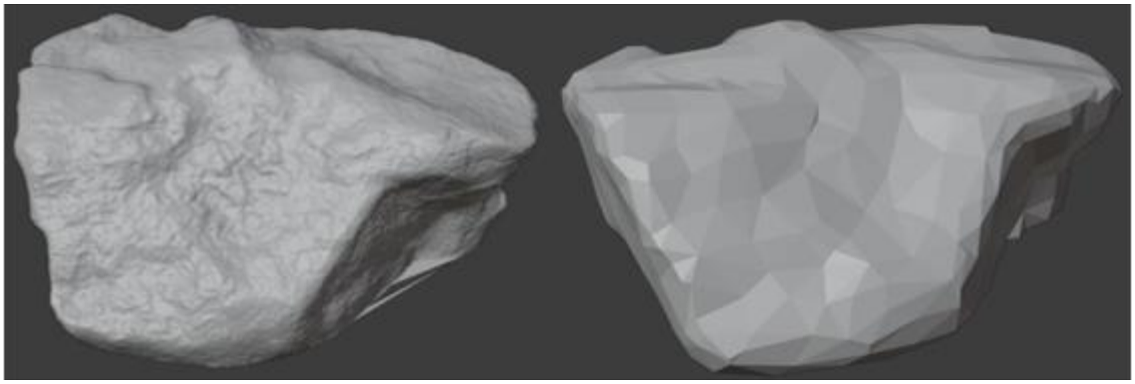

Figure 5. Full complexity model vs simplified model

D. CONVERSION TO CAD FILE

The final step prior to import into COMSOL is converting the .STL into a .STP file, which has been found to be the most efficient file type, and allows for additional complexity before COMSOL import failure. This process is completed via FreeCAD, where the Blender .STL file output is imported into FreeCAD and exported as a .STP.

E. FINAL MODEL VERSIONS

The results presented in this paper investigate the level of geometric complexity necessary to generate accurate synthetic datasets in the LF acoustic domain. To support this, several models comprised of varying surface detail were generated in order to compare the acoustic response datasets. See Figure 6, Figure 7 and Figure 8 which show the model with progressively smaller surface facets resolved within the COMSOL geometry builder. Figure 8, the highest complexity model, required manually adjustment to repair the geometry errors before solving.

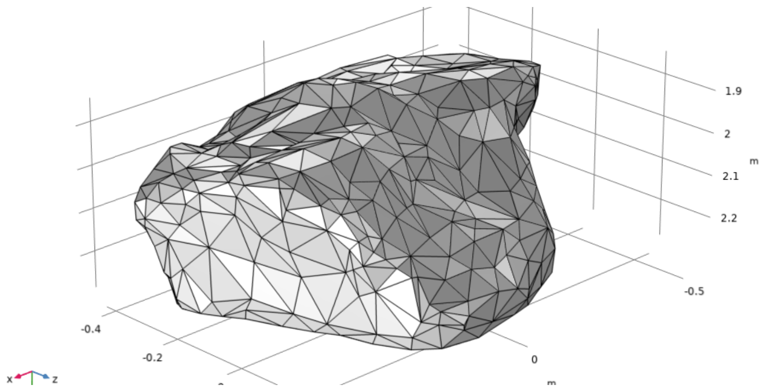

Figure 6. Most simple rock model within COMSOL

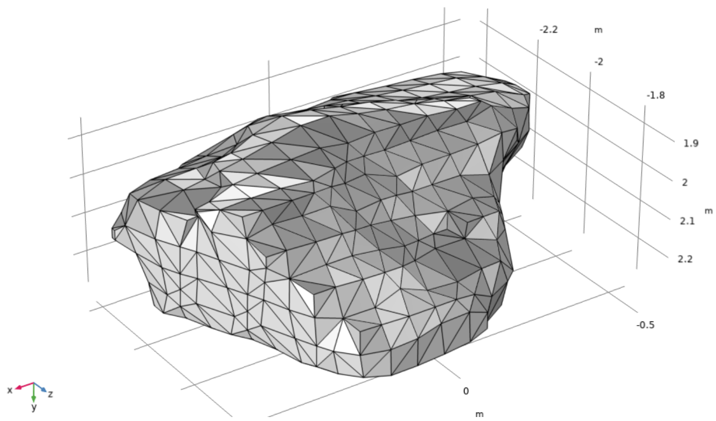

Figure 7. Moderately complex rock model within COMSOL

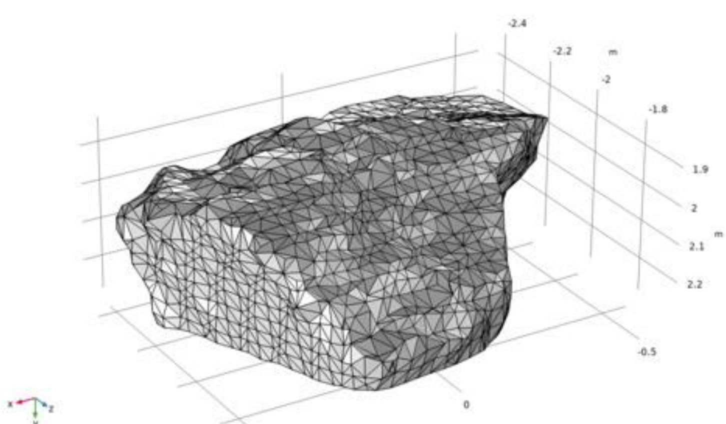

Figure 8. Most complex rock model within COMSOL

3. ACOUSTIC MODELLING

The methodology used to predict the acoustic scattering response of an arbitrary object is described in this section. The modelling approach is implemented using COMSOL Multiphysics, with post-processing of the data performed using MATLAB routines to interact directly with the solved COMSOL models via the LiveLink interface. Extensive verification and validation has been carried out against analytic solutions for scattering from acoustically-hard [2], soft [3] and elastic objects [4]; against open-literature publications of acoustic models from other institutions [5], and against experimental sonar measurements during customer-funded research programmes.

Using COMSOL's CAD Import package, the geometry contained in the .STP file is read into the Multiphysics software. The integrated geometry builder displays the imported CAD file, which allows any minor flaws in the geometry to be manually repaired if necessary.

Once the desired geometry has been set up, several remaining aspects of the modelling process must be configured; these are underlying physics, material properties, meshing and the numerical solver to be used.

The equations which must be solved are the Helmholtz equation, which governs the acoustic pressure field in the fluid surrounding the object of interest, and the constitutive equations within the solid object itself, which relate stress to strain. The pressure field is formulated as a background field consisting of an infinite plane wave at a single monochromatic frequency, plus a scattered component resulting from the interaction of this plane wave with the object of interest. On the exterior surface of the object, where the fluid and solid domains are in contact, coupling between the two physics regimes is enforced by specifying a structural-acoustic boundary. These boundary conditions equate the second time-derivative of the elastic deformation of the object to the forcing resulting from the acoustic pressure field. For the results presented in this paper, it is further assumed that the surrounding external acoustic domain is homogeneous and infinite in extent. However, in a more general context, the effect of target proximity to a (poro-)elastic seabed are captured via a modified set of boundary conditions.

In order to fully specify the structural-acoustic coupling, material properties for all regions of the modelled geometry are required. For the fluid medium, these are sound speed and density – note also that the model captures the effect of fluid-filled interior cavities and voids, although these must be included separately to the exterior fluid within the modelling workflow. In solid regions, the required material parameters are density, Young's modulus and Poisson's ratio (or equivalently, compressional- and shear-wave speeds).

Following configuration of the physics and material properties, the imported CAD geometry must be discretized into a set of tetrahedral mesh elements where the numerical solution is to be calculated. This is done via a Delaunay triangulation procedure in which the maximum allowable element size is constrained. The size threshold used is 8 mesh elements per wavelength, with a range between 6 and 16 elements per wavelength reported in the literature by other authors. This constraint is also applied to the minimum mesh element size, to avoid computational inefficiencies due to the presence of unnecessarily small mesh elements. The effect of this constraint is to prevent numerical errors from occurring by ensuring that phase differences across all regions of the modelled geometry are adequately resolved. Note additionally that this constraint is applied to the shear-wave parameters, which are typically slower than compressional waves and hence require a denser mesh. Figure 9 compares the underlying imported geometry with the mesh of solution nodes.

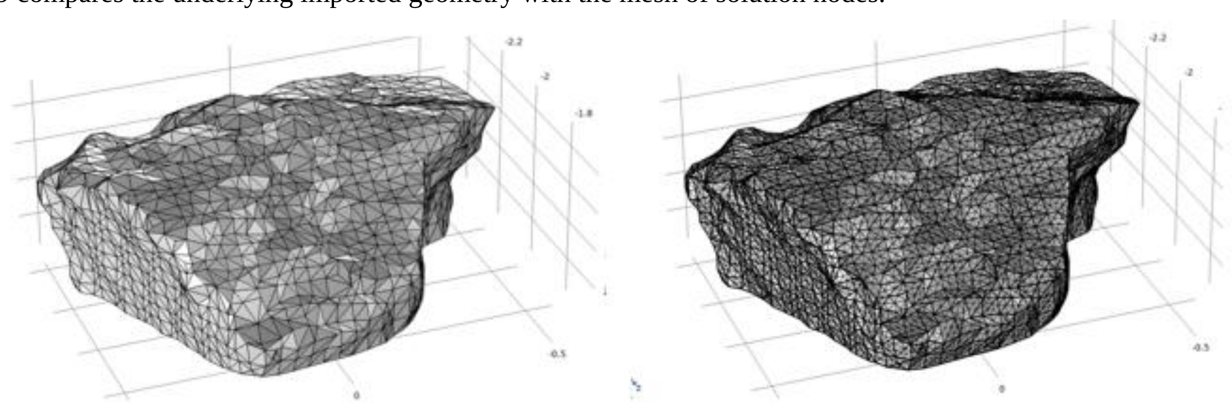

Figure 9. A comparison of the imported CAD file (left) and the discretised mesh on which the equations are solved (right)

In solving the model, a coupled FEM-BEM formulation is used, with both components defined in the frequency domain. The finite element method (FEM) component of the model is applied to the internal elastic problem, which explicitly solves for the vector displacement in all solid, linearly-elastic domains. Conversely, the acoustic component of the problem is formulated using the boundary element method (BEM) to solve for the pressure in the exterior fluid. This allows the solution to be defined everywhere in the free-field outside of the scattering object without explicitly needing to apply a mesh to the surrounding space. The key advantage of this approach is that a wider frequency range can be captured, compared to a coupled acoustic FEM – elastic FEM approach. One exception to this method is the treatment of any internal fluid-filled cavities, for which an acoustic FEM approach is used (with the same acoustic-elastic coupling routine as used for the boundary element model).

Since the model is solved in the frequency domain, the simulation must be executed for a set of discrete frequencies across the band of interest, with a final inverse Fourier transform to the time-domain if desired. This is done by performing a batch sweep across the frequency band, which results in a separate model file for each solution frequency (and so makes the procedure more robust against crashes). Within each model file, the direction of the plane wave is scanned through 360o in small increments, in order to predict the directional response of the scattering object. In the results presented in this paper, the direction of the incident plane wave is constrained to lie in the same horizontal plane as the modelled target, although an elevation angle can be specified if needed by adding a vertical component to the background pressure field. An example of the scattered pressure field is given in Figure 10.

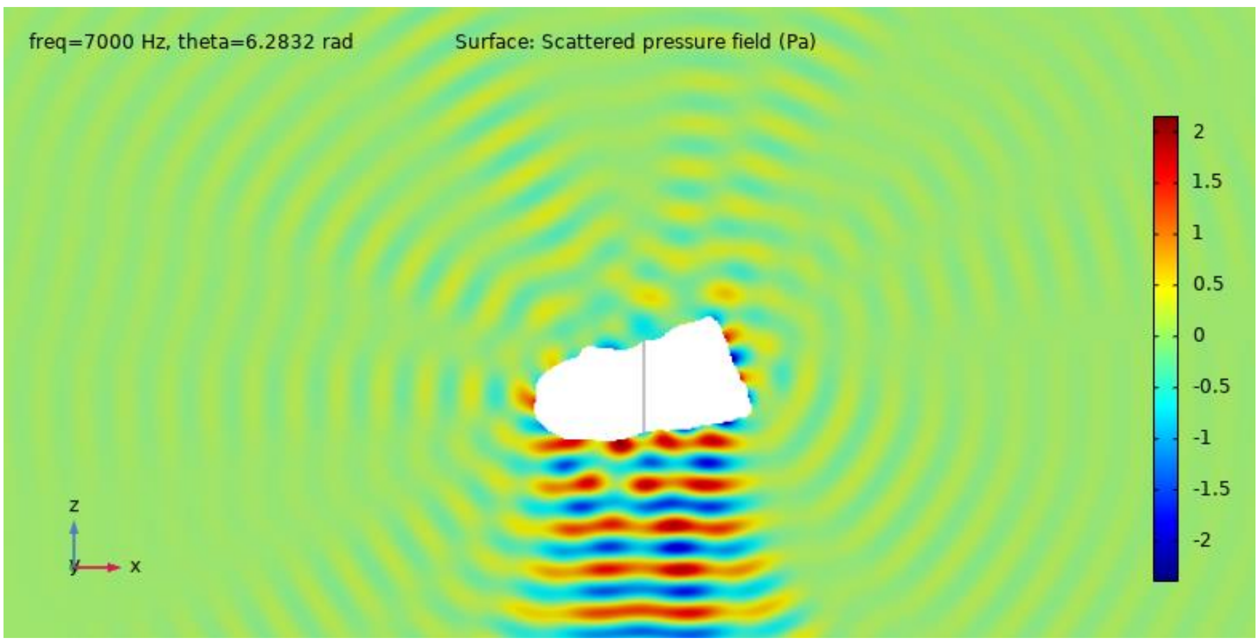

Figure 10. The scattered pressure field resulting from insonification by a 7 kHz plane wave propagating from the top of the page. Multiple bistatic reflections plus a shadow zone are visible.

Once solved for all required frequencies and incidence angles (also known as aspect angles), a MATLAB-based post-processing routine is used to interrogate the model files in an automated manner. This involves reading in the model file for each frequency, calculating the backscattered pressure for each direction of incidence, and exporting the results in CSV format. Finally, the backscattered pressure is converted to dB (relative to 1Pa at 1m) and is displayed as colour data on a 2D plot, where the horizontal axis indicates direction of incidence and the vertical axis denotes frequency. This type of display, as typified by Figure 11, is termed a frequency-aspect (FrAs) plot of Target Echo Strength (TES), which provides a complete and concise description of the acoustic characteristics of the object of interest, including resonant behaviour which results in extension of the echo in the time-domain.

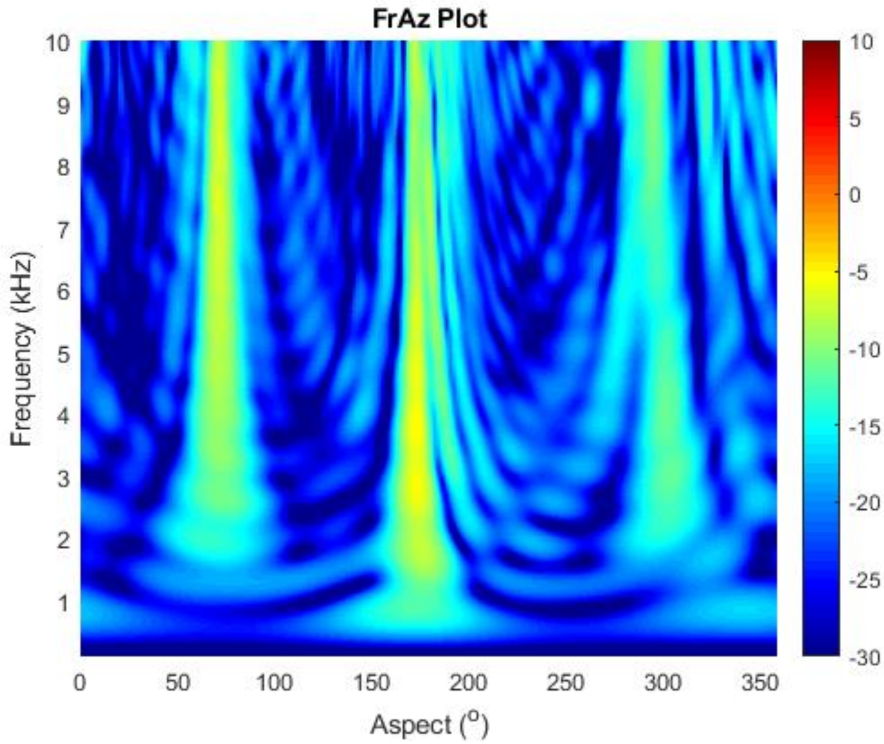

Figure 11. A frequency-aspect plot showing the predicted TES of the rock reconstructed using photogrammetry, corresponding to the model geometry shown in Figure 6

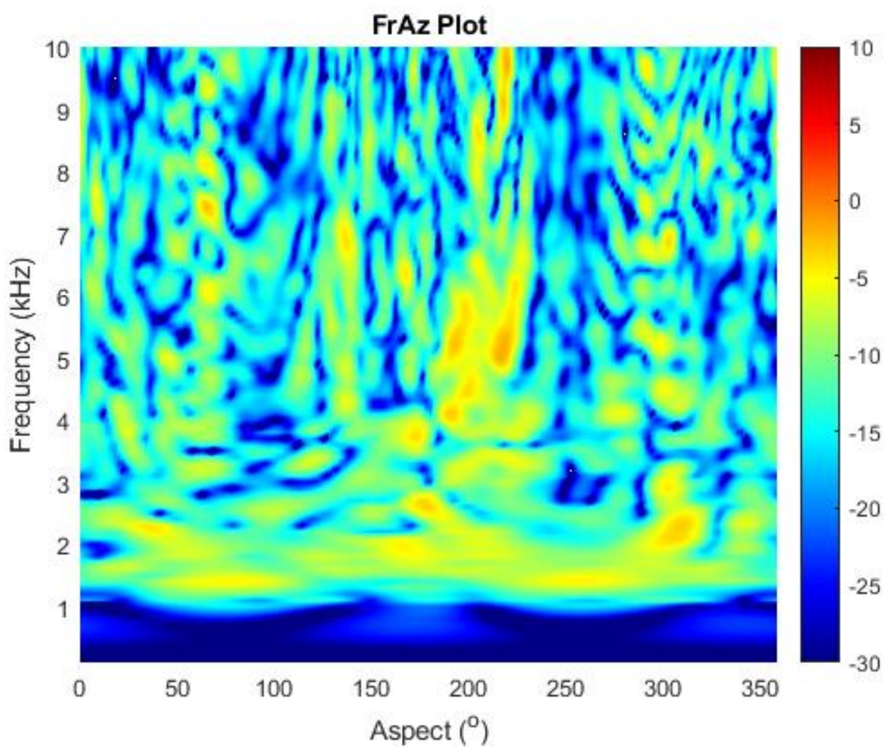

Figure 12. A frequency-aspect plot showing the predicted TES of the rock reconstructed using photogrammetry, corresponding to the model geometry shown in Figure 7

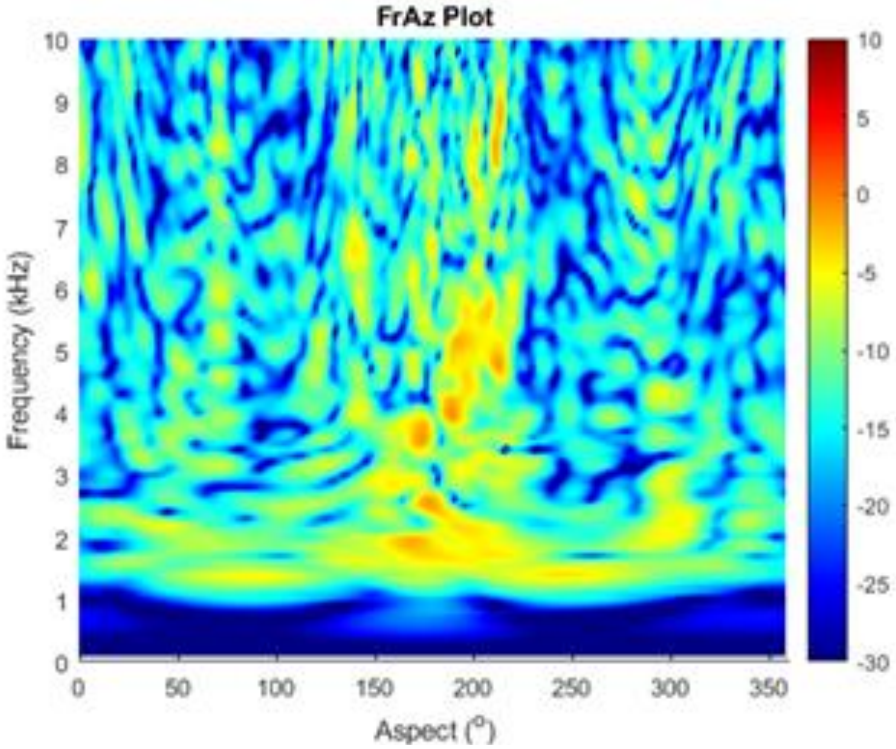

Figure 13. A frequency-aspect plot showing the predicted TES of the rock reconstructed using photogrammetry, corresponding to the model geometry shown in Figure 8

Figures 11-13 show a set of three FrAs plots, with Figure 11 corresponding to the simplest rock geometry and the Figure 13 representing scattering from the most complex rock mode. It can be seen that there are significant differences between the first two plots, suggesting that the most simplified geometry did not contain adequate surface detail to fully capture the scattering properties. Conversely, the close similarity between the last two plots indicates that the moderately complex model was able to sufficiently represent the object.

4. CONCLUSION

During the study presented in this paper, an approach for modelling the interaction of irregularly-structured objects with a sound field has been devised. Using photogrammetry software, images of a large rock were used to demonstrate that it is possible to represent the geometry of a natural object, with fractal surface roughness unsuitable for reproduction by an experienced CAD user, in modelling space. Using multiphysics software to apply the Finite/Boundary-Element method, it was shown that the acoustic echo structure of a complex and irregular object could be predicted, and that the level of detail achieved during the photogrammetry stage was sufficient to capture the most important components of the acoustic response.

REFERENCES

[1] 3DFLOW 3DF Zephyr User Manual Version 4.5
[2] Sound, Structures and Their Interaction, Junger, M. C and Feit, D, Second Edition, 1986, MIT Press, pp. 318 - 321
[3] Theoretical Acoustics of Underwater Structures, Skelton, E. A and James, J. H, 1997, Imperial College Press, pp. 88 – 92
[4] Sound Scattering by Cylinders of Finite Length, II: Elastic Cylinders, Stanton, T. K, 1986, J. Acoust. Soc. Am. 83 (1)
[5] BeTSSi IIb: A Submarine Target Strength Modelling Workshop, Nijhof, M et al, 2017, UACE Conference Proceedings